INORGANIC CHEMISTRY FRONTIERS

RESEARCH ARTICLE

View Article Online
View Journal | View Issue



Cite this: *Inorg. Chem. Front.*, 2025, **12**, 4376

# Multilayered double perovskite ferroelectric for green high-performance self-powered X-ray detection†

Zhangtong Han,[a,b,c] Qianwen Guan,[a,b,c] Huang Ye,*[a,b] Yi Liu,[a,b,c] Jianbo Wu,[a,b] Lijun Xu,[a,b,c] Chengshu Zhang,[a,b] Hang Li,[a,b,c] Qiuxiao Yin[a,b] and Junhua Luo *[a,b,c]

Received 29th November 2024,
Accepted 4th February 2025

DOI: 10.1039/d4qi03059a

rsc.li/frontiers-inorganic



Layered hybrid perovskite ferroelectrics have made significant strides in high-performance X-ray detection, attributed to their polarization-induced large built-in electric fields and excellent carrier mobility. However, most reported layered hybrid perovskite ferroelectrics rely on environmentally hazardous lead halides, which limits their broader application. Recently developed hybrid double perovskites offer promising alternatives for green self-driven X-ray detection. Herein, we explore the bulk photovoltaic effect in a two-dimensional multilayered double perovskite ferroelectric $CHMA_2CsAgBiBr_7$ (**CCAB**, $CHMA^+$ = cyclohexylmethylammonium) for self-driven X-ray detection. Due to its multilayer structure, **CCAB** exhibits a large $\mu\tau$ product of $3.3 \times 10^{-3}$ $cm^2$ $V^{-1}$, which is comparable to the three-dimensional double perovskite $Cs_2AgBiBr_6$. Specifically, the X-ray detector exhibits a photovoltage of 0.84 V under X-ray irradiation, ensuring the capability to convert X-rays into electric signals without bias. Additionally, **CCAB** exhibits a high sensitivity up to 120 μC $Gy^{-1}$ $cm^{-2}$ and a low detection limit down to 103 nGy $s^{-1}$ in the self-driven mode. Our work highlights the potential of lead-free multilayered double perovskite ferroelectrics for achieving high-performance self-driven X-ray detection, paving the way for practical applications of layered hybrid perovskite ferroelectrics in this field.

## Introduction

Direct X-ray detectors, which can directly convert X-rays into electrical signals, play an important role in applications such as medical diagnostics, safety inspections, and material analysis.[1–6] In recent years, lead halide perovskites (LHPs) have garnered considerable attention and achieved significant advancements in X-ray detection due to their easy synthesis, high X-ray absorption and excellent carrier mobility.[7,8] For instance, Song *et al.* developed an X-ray detector based on three-dimensional perovskite single crystals $MAPbI_3$ (MA = $CH_3NH_3^+$) achieving a sensitivity of up to $5.2 \times 10^6$ μC $Gy^{-1}$ $cm^{-2}$.[9] Two-dimensional (2D) multilayer LHPs, which possess a two-dimensional quantum well structure to suppress ion migration and combine the excellent semiconductor properties of three-dimensional halide perovskites, have emerged as a promising option for achieving high-performance X-ray detection.[10–16] For instance, a multilayer perovskite (BDA)$(MA)_2Pb_3Br_{10}$ (BDA = $NH_3C_4H_8NH_3^{2+}$) demonstrates high X-ray detection performance with a high sensitivity of 1984 μC $Gy^{-1}$ $cm^{-2}$ at 55.6 V $mm^{-1}$ and a low detection limit of 28.12 nGy $s^{-1}$ at 22.2 V $mm^{-1}$.[17] Despite these advances, most of these materials require operation under a high external electric field, resulting in significant ion migration and energy consumption.[18–22] Therefore, developing detectors that can detect X-ray signals without external bias is very urgent.

2D multilayer LHP ferroelectrics which combine spontaneous polarization, excellent absorption coefficients and good charge transport have emerged as promising candidates for realizing high-performance self-driven X-ray detection.[23] Notably, the bulk photovoltaic effect (BPVE) in these materials can create a built-in electric field to spontaneously and efficiently separate photo-generated carriers without the need for external bias, thereby enabling self-driven detection. For instance, Jiang *et al.* developed a high-performance self-driven X-ray detector utilizing a 2D multilayer LHP ferroelectric $(BA)_2(EA)_2Pb_3I_{10}$ (BA = $NH_3C_4H_9^+$ and EA = $CH_3CH_2NH_3^+$), which has a sensitivity of 391 μC $Gy^{-1}$ $cm^{-2}$.[24] Despite the superior performance of 2D multilayer lead components, these materials contain toxic lead, posing a significant threat to

[a]*State Key Laboratory of Functional Crystals and Devices, Fujian Institute of Research on the Structure of Matter, Chinese Academy of Sciences, Fuzhou, Fujian, 350002, P. R. China. E-mail: yehuang@fjirsm.ac.cn, jhluo@fjirsm.ac.cn*
[b]*State Key Laboratory of Structure Chemistry, Fujian Institute of Research on the Structure of Matter, Chinese Academy of Sciences, Fuzhou, Fujian, 350002, P. R. China*
[c]*University of Chinese Academy of Sciences, Beijing, 100049, China*
† Electronic supplementary information (ESI) available. See DOI: https://doi.org/10.1039/d4qi03059a

human health. To address this issue, it is imperative to develop X-ray detection methods utilizing lead-free halide perovskites, thereby achieving environmentally friendly self-driven X-ray detectors with high performance.

As environmentally friendly alternatives, 2D lead-free multilayer double halide perovskite ferroelectrics are considered promising candidates for green self-driven X-ray detection, owing to their non-toxic, excellent carrier transport properties and possession of spontaneous polarization.[25] Xu *et al.* developed an X-ray detector based on a multilayer double perovskite $BA_2CsAgBiBr_7$.[26] Benefiting from its multi-layer structure, it exhibits excellent carrier transport properties, showing great promise for high-performance self-driven X-ray detection. Similar to 2D multilayer LHP ferroelectrics, 2D multilayer double halide perovskite ferroelectrics have spontaneous polarization-induced bulk photovoltaic effects, which are anticipated to facilitate self-driven X-ray detection. Yao *et al.* reported a high-curie temperature multilayered hybrid double perovskite $(C_6H_5CH_2NH_3)_2CsAgBiBr_7$,[37] which are anticipated to facilitate self-driven X-ray detection at room temperature. However, due to the limited availability of multilayer double halide perovskite ferroelectrics, no 2D multilayered double halide has been applied to self-driven X-ray detection. Consequently, we posit that utilizing lead-free multilayer perovskite ferroelectrics represents an effective strategy for achieving high-performance self-driven X-ray detection.

In this work, a high-quality single-crystal X-ray detector based on a 2D lead-free double perovskite ferroelectric $CHMA_2CsAgBiBr_7$ (**CCAB**, $CHMA^+$ is cyclohexylmethylammonium) was constructed. Owing to the merits of its multilayered structure, **CCAB** has a large $\mu\tau$ product of $3.3 \times 10^{-3}$ $cm^2$ $V^{-1}$ and good X-ray absorption, which facilitates high-performance X-ray detection. Specifically, due to the BPVE of **CCAB**, the single crystal device can spontaneously separate and transport photogenerated carriers without external bias, thereby imparting self-driven detection capabilities to **CCAB**. Based on these merits, the **CCAB**-based device exhibits a great sensitivity of 120 μC $Cy^{-1}$ $cm^{-2}$ and a low detection limit of 103 nGy $s^{-1}$ at 0 V. Moreover, **CCAB** achieves a high sensitivity of 3312 μC $Gy^{-1}$ $cm^{-2}$ under a bias of 100 V, outperforming most 2D halide double perovskites. This work successfully achieved high-performance self-driven X-ray detection in multilayer lead-free halide double perovskite ferroelectrics, offering a promising pathway for the development of environmentally friendly self-driven X-ray detectors.

## Results and discussion

Single crystals (SC) of **CCAB** were grown from a hydroiodic acid solution using a slow cooling process (Fig. 1a). Powder X-ray diffraction (PXRD) patterns from simulation and experimental measurement confirm the phase purity (CCDC 2203833, Fig. 1b),[27] and the X-ray pattern of the **CCAB** SC shows well-defined (*h*00) diffraction peaks, which indicate its high quality and high orientation. The thermogravimetric (TG) curve (Fig. S1†) indicates that the decomposition temperature of **CCAB** is as high as 555 K, demonstrating its high thermal

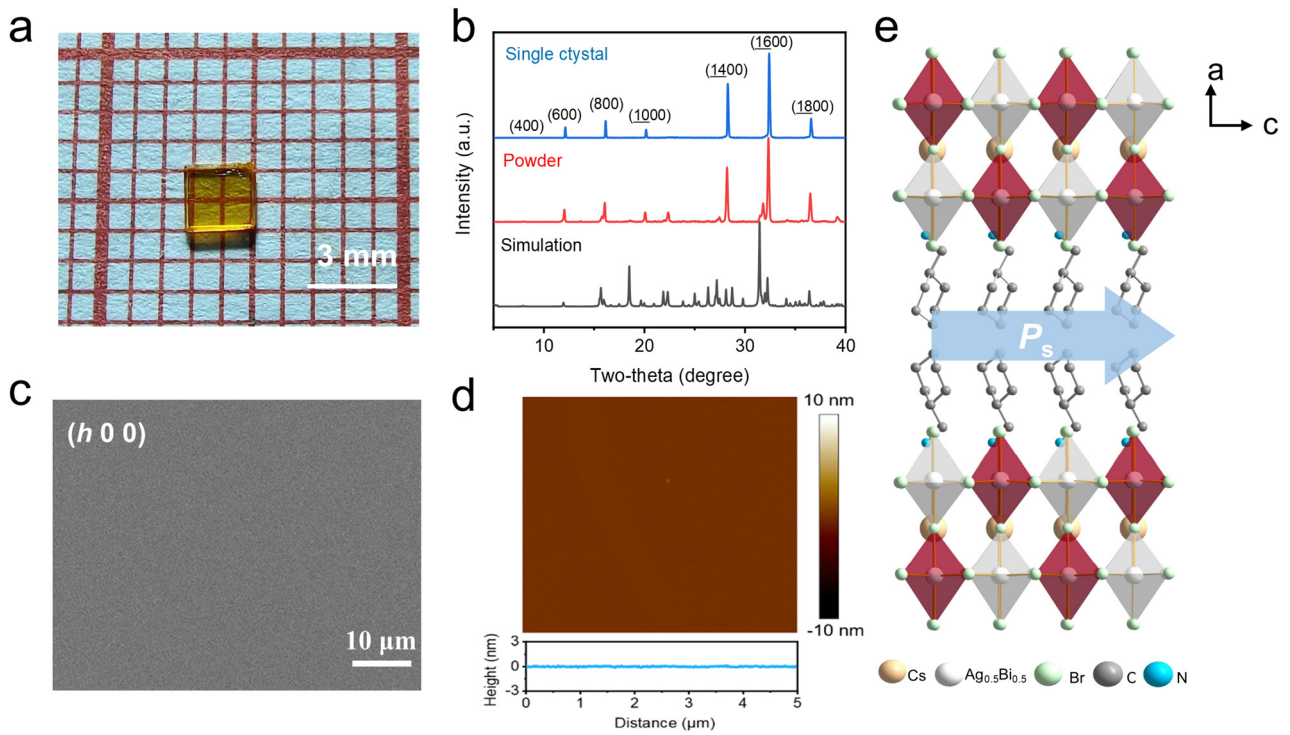


**Fig. 1** (a) The high-quality crystal image of the **CCAB** single crystal. (b) XRD measurement of the powder and crystal. (c) The SEM image of **CCAB**. (d) The AFM image of **CCAB**. (e) The crystal structure of **CCAB**. The white color shows the atomic co-occupancy of Ag and Bi.

stability. Scanning electron microscopy (SEM) and atomic force microscopy (AFM) were used to characterize the surface morphology of the crystal. As illustrated in Fig. 1c and d, the surface of the crystals is flat and smooth with no obvious defects, which affirms the high quality of the **CCAB** SC. Through analysis of the AFM data, the root mean square roughness (RMS) of the crystallographic plane was determined to be 0.243 nm, indicating the high quality of the **CABB** crystal. As depicted in Fig. 1e, **CCAB** adopts the typical 2D motif and the inorganic layer consists of two octahedral layers composed of alternating $AgBr_6$ and $BiBr_6$ octahedra, with the $Cs^+$ cation fully encapsulated in a cavity formed by corner-sharing octahedra. The presence of the heavy elements Cs, Bi, and Ag in **CCAB** is beneficial for X-ray absorption and its bilayer inorganic skeleton facilitates carrier transport, making it a potential candidate for high-performance X-ray detection. Furthermore, **CCAB** crystallizes in the polar space group *Ama*2 at room temperature. With the increase in temperature, **CCAB** further transforms into a middle phase with a centrosymmetric space group of *Cmcm* (338 K, Fig. S2a†) and finally transforms into a centrosymmetric space group of *I*4/*mmm* (378 K, Fig. S2b†). Such a symmetry-breaking form of **CCAB** obeys the Aizu rule with the notation 4/*mmmFmm*2 and its ferroelectricity along the *c*-axis has been demonstrated by the polarization *versus* electric field hysteresis loops as shown in Fig. S3.† The **CCAB**-based device shows piezoelectric response along the *c*-axis with a $d_{33}$ value of 1.6 pC $N^{-1}$, while no piezoelectric response is observed along the nonpolar axis (Fig. S4†). The ferroelectric polarization of the **CCAB** crystal along the *c*-axis generates a built-in electric field to separate the photogenerated carriers, thus giving the **CCAB** SC the ability for self-driven detection.

For efficient X-ray detection, materials must proficiently absorb X-ray photons. Therefore, to further evaluate the efficiency of absorption of X-ray photons by the **CCAB** SC, the X-ray attenuation efficiency and absorption coefficient of **CCAB** were calculated using the photon cross-section database. As illustrated in Fig. 2a, the calculated absorption coefficient of **CCAB** is larger than that of $(HIS)_2AgBiBr_8$ (HIS = histammonium) and crystalline Si, but comparable to that of α-Se. Conversely, Fig. 2b depicts the thickness of these materials as a function of the 50 keV X-ray photon attenuation efficiency. The **CCAB** material attenuates over 78% of the X-ray photons at a thickness of 1.0 mm, which is significantly higher than that of Si (≈8.6%). The charge collection of **CCAB** is another key factor influencing the performance of X-ray detection, which can be evaluated by the carrier mobility lifetime ($\mu\tau$). Consequently, we derived the $\mu\tau$ product by fitting photocurrent–voltage curves according to the modified Hecht equation:[1]

$$I = \frac{I_0 \mu\tau V}{L^2}\left[1 - \exp\left(\frac{-L^2}{\mu\tau V}\right)\right] \quad (1)$$

where $I$ is the photocurrent, $I_0$ is the saturated photocurrent, $L$ is the distance between electrodes, and $V$ is the applied bias. As

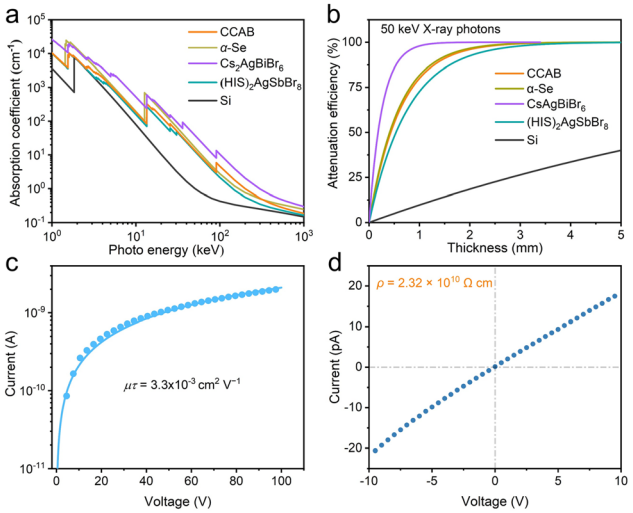


**Fig. 2** (a) The X-ray absorption spectra of **CCAB**. (b) Attenuation efficiency of **CCAB** to 50 keV X-ray photons *versus* thickness. (c) The $\mu\tau$ product of **CCAB** along the *c*-axis of the polarization direction. (d) The bulk resistivity of the **CCAB** SC.

shown in Fig. 2c, the $\mu\tau$ product of the **CCAB** SC is up to 3.3 × $10^{-3}$ $cm^2$ $V^{-1}$ under X-ray irradiation, which is larger than those of the reported lead-free perovskite X-ray detectors, such as $(4F\text{-}PEA)_2AgBiBr_8$ (2.9 × $10^{-5}$ $cm^2$ $V^{-1}$, 4F-PEA = 4-fluorophenethylammonium),[28] $[(R/S\text{-}PPA)_4(n\text{-}BA)_6Ag_2Bi_4I_{24}]\cdot 2H_2O$ (2.24 × $10^{-4}$ $cm^2$ $V^{-1}$, *R*/*S*-PPA = *R*/*S*-1-phenylpropylamine)[29] and $(4,4\text{-}DFPD)_4AgSbI_8$ (6.19 × $10^{-4}$ $cm^2$ $V^{-1}$, 4,4-DFPD = 4,4-difluoropiperidinium),[30] and much higher than that of the commercial α-Se film detector (≈$10^{-7}$ $cm^2$ $V^{-1}$). Additionally, resistivity is also an important parameter for X-ray detectors. The bulk resistivity of the **CCAB** SC along the *c*-axis can be calculated as 2.32 × $10^{10}$ Ω cm (Fig. 2d). This value is comparable to those of many lead-free halide double perovskites, such as $(I\text{–}C_4H_8NH_3)_4AgBiI_8$ (3.04 × $10^{10}$ Ω cm)[31] and $(PEA)_4AgBiBr_8$ (6.77 × $10^{10}$ Ω cm, PEA = phenethylammonium).[28] The high resistivity of the **CCAB** SC will facilitate the reduction of dark current and suppression of current noise, which is essential for improving the X-ray detection performance.

Importantly, **CCAB** exhibits ferroelectricity, which leads to spontaneous polarization to separate photogenerated carriers, thus enabling self-driven detection. To further investigate the self-driven detection capabilities of **CCAB**, we fabricated vertical electrodes Ag/**CCAB** SC/Ag parallel to the polar *c*-axis direction (Fig. 3a). The absorption onset of **CCAB** occurs at a wavelength of 569 nm according to the ultraviolet-visible absorption (Fig. S5†); therefore we studied its BPVE under 405 nm light. Under 405 nm illumination, an open-circuit photovoltage of 0.5 V can be obtained from the current–voltage curves of the **CCAB** SC device (Fig. 3b). Similarly, **CCAB** exhibits a photovoltage up to 0.85 V under X-ray irradiation as shown in Fig. 3c. Such a bulk photovoltage is larger than many reported bulk photovoltages in lead-free hybrid perovskites, such as $(R\text{-}MPA)_4AgBiI_8$ (0.36 V, *R*-MPA = *R*-β-methylphenethylammonium),[32] $(BZA)_2(R/$

 

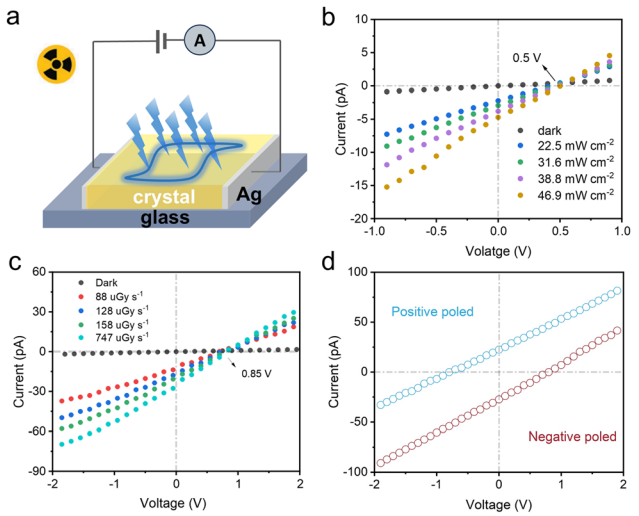


**Fig. 3** (a) Schematic of the X-ray detector with electrodes oriented parallel to the polar *c*-axis made from the **CCAB** single crystal. (b) The current–voltage traces of the **CCAB** device under 405 nm light illumination. (c) The current–voltage traces of the **CCAB** device under different X-ray irradiation. (d) Dependence of the photocurrent direction on the polarization direction (the upper and lower parts of the figure correspond to the direction of the current after positive poling and negative poling, respectively).

*S*-PPA)$BiI_6$ (0.4 V, BZA = benzylamine) and (*R*/*S*-PPA)$_2BiI_5$ (0.63 V),[33] which has the merit of enabling high-performance self-driven X-ray detection. To further demonstrate the BPVE of the **CCAB** device, a study was conducted to determine whether the spontaneous polarization of **CCAB** would result in the corresponding flipping in response to changes in the polarization electric field. As shown in Fig. 3d, the open-circuit voltage and short-circuit current of **CCAB** have been identified as −0.83 V/+22.5 pA and +0.85 V/−23 pA, respectively, following positive and negative polarization. These results indicate that the BPVE of the **CCAB** SC originates from spontaneous polarization, thus enabling **CCAB** with self-driven detection capability. In summary, the good X-ray absorption, large carrier mobility and BPVE of **CCAB** provide a suitable platform for achieving high-performance self-driven X-ray detection.

Hence, we further investigated the response of the **CCAB** SC detectors to X-rays. Due to the BPVE induced by ferroelectricity, an obvious response of the device to X-rays at 0 V bias can be observed as shown in Fig. 4a. As the X-ray dose increases from 4.35 to 87.66 μGy $s^{-1}$, the photocurrent density of the **CCAB** device shows a linear increase from 4.04 to 19.39 nA $cm^{-2}$, indicating excellent X-ray response. This device also exhibits a strong X-ray response under external bias voltages from 10 V to 100 V as shown in Fig. S6–S10.† As depicted in Fig. 4b and c, the sensitivity under different bias voltages and doses is obtained by linearly fitting the current density and X-ray dose rate. The high sensitivity of **CCAB** is up to 120 μC $Gy^{-1}$ $cm^{-2}$ under zero bias, which is higher than those of other lead-free hybrid perovskites such as (BZA)$_2$(*R*/*S*-PPA)$BiI_6$ (53.2 μC $Gy^{-1}$ $cm^{-2}$ at 0 V bias), (*R*/*S*-PPA)$_2BiI_5$ (0.31 μC $Gy^{-1}$ $cm^{-2}$ at 0 V bias),[33] (*R*-MPA)$_4AgBiI_8$ (40 μC $Gy^{-1}$ $cm^{-2}$ at 0 V bias),[32] *etc*. Pleasantly, the sensitivity of **CCAB** is much higher than that of a conventional inorganic material α-Se film detector (20 μC $Gy^{-1}$ $cm^{-2}$ at 2000 V bias). Moreover, the detector also exhibits excellent X-ray response under external bias. As the external bias voltage increases, the sensitivity increases from 517 μC $Gy^{-1}$ $cm^{-2}$ (10 V bias) to 3312 μC $Gy^{-1}$ $cm^{-2}$ (100 V bias), which is larger than those of most currently available 2D lead-free double perovskite detectors, such as (HIA)$_2AgBiBr_8$ (118 μC $Gy^{-1}$ $cm^{-2}$, 10 V bias, HIA = histamine),[34] (4,4-DFPD)$_4AgBiI_8$ (188 μC $Gy^{-1}$ $cm^{-2}$, 50 V bias)[35] and (4-AP)$_2AgBiBr_8$ (1117.3 μC $Gy^{-1}$ $cm^{-2}$, 80 V bias, 4-AP = 4-amidinopyridine).[36] The detection limit is another critical factor for X-ray detectors. According to The International Union of Pure and Applied Chemistry, the detection limit is the X-ray dose rate when the signal-to-noise (SNR) ratio is equal to 3. The SNR value can be measured using the following equation:

$$\mathrm{SNR} = \frac{\overline{I_{\mathrm{photo}}} - \overline{I_{\mathrm{dark}}}}{\sqrt{\frac{1}{N}\sum_{i}^{N}\left(I_{\mathrm{i}} - \overline{I_{\mathrm{photo}}}\right)^2}} \quad (2)$$

where $\overline{I_{\mathrm{photo}}}$ denotes the average photocurrent, $\overline{I_{\mathrm{dark}}}$ denotes the average dark current, and $I_{\mathrm{i}}$ denotes the measured photocurrent. As illustrated in Fig. 4d, the detection limit is 103 nGy $s^{-1}$ for the device at zero bias, significantly lower than the current dose rate of the standard medical diagnostic dose (5.5 μGy $s^{-1}$). The detection limit of the **CCAB** SC under 100 V bias was also calculated as shown in Fig. S11.† The detection limit under 100 V bias (798 nGy $s^{-1}$) is higher than that of **CCAB** under 0 V bias, due to increased dark current and noise resulting from significant ion migration under elevated external bias voltage. In addition, the long-term operational and environmental stability of the device is critical in practical applications. The stability of the dark current is an important parameter of X-ray detectors, which can be calculated from the following equation:

$$I_{\mathrm{drift}} = \frac{(I_t - I_0)}{E \times A \times t} \quad (3)$$

where $I_0$ and $I_t$ are the currents at the start and time $t$, respectively, $E$ is the electric field, and $A$ is the device area. As shown in Fig. 4e, there is almost no dark current drift in the self-driven mode compared to a dark current drift of 3.7 $10^{-7}$ nA $cm^{-1}$ $s^{-1}$ $V^{-1}$ at 10 V bias, which indicates that the device maintains a highly stable baseline at 0 V bias. To evaluate the stability of this device, we assessed the X-ray response of the detector under continuous X-ray radiation with a dose rate of 1.58 mGy $s^{-1}$. The photocurrent and dark current did not significantly change at a total X-ray dosage of 793 mGy, demonstrating its excellent radiation stability (Fig. 4f). Finally, the environmental stability of the **CCAB** device is evaluated at 0 V bias. As shown in Fig. 4g, after being exposed to air for three months, PXRD shows that the **CCAB** crystal exhibited no significant phase change. Moreover, the detector retains excep-

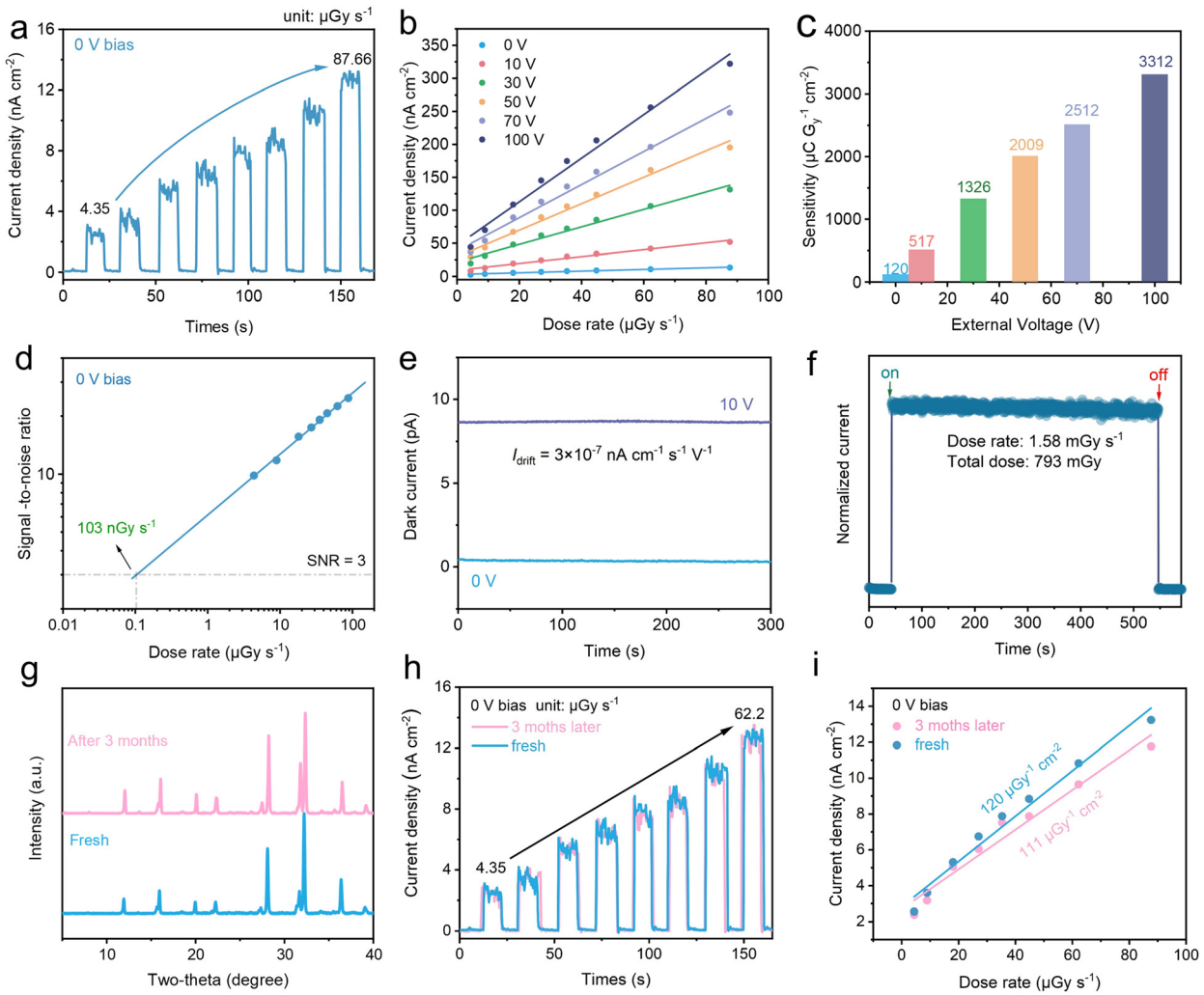


**Fig. 4** (a) X-ray response under different dose rates at 0 V bias. (b) Dose rate-dependent X-ray response of the **CCAB** SC device under different voltages. (c) The sensitivities of devices based on **CCAB** under different bias voltages. (d) The SNR of the **CCAB** device at 0 V bias. (e) Dark current drift under 0 and 10 V bias, respectively. (f) Photocurrent stability of the **CCAB** SC detector under continuous X-ray irradiation. (g) PXRD patterns of the original **CCAB** sample and after three months. (h) The irradiation response stability is measured after three months at 0 V bias. (i) Comparison of sensitivity of the original **CCAB** sample and after three months at 0 V bias.

tional operational stability after three months and the photoresponse to X-ray is only weakly degraded (Fig. 4h). As depicted in Fig. 4i, approximately 92% (111 μC $Gy^{-1}$ $cm^{-2}$) of the initial sensitivity was still maintained at 0 V bias after three months in air (≈298 K, ≈48.6% RH). This result confirms the excellent environmental stability of the device. This study demonstrates that multilayered double perovskite ferroelectrics with radiation photovoltages are a class of potential materials for high-performance self-driven X-ray detection.

## Conclusions

In conclusion, we successfully synthesized high-quality crystals of a 2D lead-free perovskite ferroelectric $CHMA_2CsAgBiBr_7$ (**CCAB**) and further constructed a high-performance X-ray detector based on **CCAB**. Due to the BPVE resulting from the ferroelectricity of **CCAB**, the single crystal device can drive the separation and transport of charge carriers without bias, thus allowing **CCAB** to have self-driven detection capability. Furthermore, owing to the merits of its multilayered structure, **CCAB** has a large $\mu\tau$ product of $3.3 \times 10^{-3}$ $cm^2$ $V^{-1}$, which facilitates the collection of carriers. Under zero bias, **CCAB** showed a considerable sensitivity of 120 μC $Cy^{-1}$ $cm^{-2}$ and a low detection limit of 103 nGy $s^{-1}$. Moreover, the sensitivity of **CCAB** reaches as high as 3312 μC $Gy^{-1}$ $cm^{-2}$ under 100 V bias, which is higher than those of most 2D halide double perovskites. This work successfully achieved high-performance self-driven X-ray detection in multilayered lead-free halide double perovskite ferroelectrics, offering a promising pathway for developing environmentally friendly self-driven X-ray detectors.

 

## Data availability

The data supporting this article have been included as part of the ESI,† including additional computational details and experimental details, materials and methods, crystal morphology, crystal structure data, PXRD patterns, the TG curve, basic photoelectric properties, and X-ray detection performance.

## Conflicts of interest

The authors declare no conflict of interest.

## Acknowledgements

This work was financially supported by the National Natural Science Foundation of China (22435005, 22193042, 22125110, and U21A2069), the Key Research Program of Frontier Sciences of the Chinese Academy of Sciences (ZDBS-LY-SLH024), and the Youth Innovation Promotion of Chinese Academy of Sciences (2019301, Y202069, and 2020307).

## References

1 Y. C. Kim, K. H. Kim, D.-Y. Son, D.-N. Jeong, J.-Y. Seo, Y. S. Choi, I. T. Han, S. Y. Lee and N.-G. Park, Printable organometallic perovskite enables large-area, low-dose X-ray imaging, *Nature*, 2017, **550**, 87–91.
2 H. Wu, Y. Ge, G. Niu and J. Tang, Metal Halide Perovskites for X-Ray Detection and Imaging, *Matter*, 2021, **4**, 144–163.
3 Y. Zhou, J. Chen, O. M. Bakr and O. F. Mohammed, Metal Halide Perovskites for X-ray Imaging Scintillators and Detectors, *ACS Energy Lett.*, 2021, **6**, 739–768.
4 J. Jiang, M. Xiong, K. Fan, C. Bao, D. Xin, Z. Pan, L. Fei, H. Huang, L. Zhou, K. Yao, X. Zheng, L. Shen and F. Gao, Synergistic strain engineering of perovskite single crystals for highly stable and sensitive X-ray detectors with low-bias imaging and monitoring, *Nat. Photonics*, 2022, **16**, 575–581.
5 Y. Wu, J. Feng, Z. Yang, Y. Liu and S. Liu, Halide Perovskite: A Promising Candidate for Next-Generation X-Ray Detectors, *Adv. Sci.*, 2022, **10**, 2204512.
6 R. Zhuang, X. Wang, W. Ma, Y. Wu, X. Chen, L. Tang, H. Zhu, J. Liu, L. Wu, W. Zhou, X. Liu and Y. Yang, Highly sensitive X-ray detector made of layered perovskite-like $(NH_4)_3Bi_2I_9$ single crystal with anisotropic response, *Nat. Photonics*, 2019, **13**, 602–608.
7 H. Wei, Y. Fang, P. Mulligan, W. Chuirazzi, H.-H. Fang, C. Wang, B. R. Ecker, Y. Gao, M. A. Loi, L. Cao and J. Huang, Sensitive X-ray detectors made of methylammonium lead tribromide perovskite single crystals, *Nat. Photonics*, 2016, **10**, 333–339.
8 S. Shrestha, R. Fischer, G. J. Matt, P. Feldner, T. Michel, A. Osvet, I. Levchuk, B. Merle, S. Golkar, H. Chen, S. F. Tedde, O. Schmidt, R. Hock, M. Rührig, M. Göken, W. Heiss, G. Anton and C. J. Brabec, High-performance direct conversion X-ray detectors based on sintered hybrid lead triiodide perovskite wafers, *Nat. Photonics*, 2017, **11**, 436–440.
9 Z. Song, A. Abate, S. C. Watthage, G. K. Liyanage, A. B. Phillips, U. Steiner, M. Graetzel and M. J. Heben, High-performance direct conversion X-ray detectors based on sintered hybrid lead triiodide perovskite wafers, *Adv. Energy Mater.*, 2016, **6**, 1600846.
10 B. Zhang, T. Zheng, J. You, C. Ma, Y. Liu, L. Zhang, J. Xi, G. Dong, M. Liu and S. Liu, Electron-Phonon Coupling Suppression by EnhancedLattice Rigidity in 2D Perovskite Single Crystals for High-Performance X-Ray Detection, *Adv. Mater.*, 2022, **35**, 2208875.
11 N. Zhou and H. Zhou, Spacer Organic Cation Engineering for Quasi-2D Metal Halide Perovskites and the Optoelectronic Application, *Small Struct.*, 2022, **3**, 2100232.
12 W. Li, M. Li, Y. He, J. Song, K. Guo, W. Pan and H. Wei, Arising Two-dimensional Perovskites for Ionizing Radiation Detection, *Adv. Mater.*, 2024, **36**, 2309588.
13 Y. Zheng, T. Niu, X. Ran, J. Qiu, B. Li, Y. Xia, Y. Chen and W. Huang, Unique characteristics of 2D Ruddlesden–Popper (2DRP) perovskite for future photovoltaic application, *J. Mater. Chem. A*, 2019, **7**, 13860–13872.
14 L. N. Quan, M. Yuan, R. Comin, O. Voznyy, E. M. Beauregard, S. Hoogland, A. Buin, A. R. Kirmani, K. Zhao, A. Amassian, D. H. Kim and E. H. Sargent, Ligand-Stabilized Reduced-Dimensionality Perovskites, *J. Am. Chem. Soc.*, 2016, **138**, 2649–2655.
15 K. Wang, C. Wu, D. Yang, Y. Jiang and S. Priya, Quasi-Two-Dimensional Halide Perovskite Single Crystal Photodetector, *ACS Nano*, 2018, **12**, 4919–4929.
16 C. Ji, Y. Li, X. Liu, Y. Wang, T. Zhu, Q. Chen, L. Li, S. Wang and J. Luo, Monolayer-to-Multilayer Dimensionality Reconstruction in a Hybrid Perovskite for Exploring the Bulk Photovoltaic Effect Enables Passive X-ray Detection, *Angew. Chem., Int. Ed.*, 2021, **60**, 20970–20976.
17 S. Wang, F. Wang, X. Xu, N. Zhang, R. Zhang, L. Lv, X. Jiang, X. Huang, S. Wu and Y. Ding, Methylammonium-based quasi-two-dimensional perovskite single crystals for highly sensitive X-ray detection and imaging, *ACS Appl. Mater. Interfaces*, 2023, **15**, 58566–58572.
18 W. Zhao and J. A. Rowlands, X-ray imaging using amorphous selenium: Feasibility of a flat panel self-scanned detector for digital radiology, *Med. Phys.*, 1998, **22**, 1595–1604.
19 C. Zhou, M. Han, Y. Xiao, W. Tan, X. Jin, X. Wu, Y. Yang, S. Zhu, H. Lin, S. Lin, Q. Chen, Q. Liang, J. Hu and W. Zhang, Y. Jiang, Lead-free perovskites and derivatives enable direct and scintillation-type X-ray detection, *Mater. Sci. Eng., R*, 2023, **156**, 100756.
20 M. Wang, W. Wang, B. Ma, W. Shen, L. Liu, K. Cao, S. Chen and W. Huang, Lead-Free Perovskite Materials for Solar Cells, *Nano-Micro Lett.*, 2021, **13**, 62.
21 S. You, P. Yu, J. Wu, Z. K. Zhu, Q. Guan, L. Li, C. Ji, X. Liu and J. Luo, Weak X-Ray to Visible Lights Detection Enabled

by a 2D Multilayered Lead Iodide Perovskite with Iodine-Substituted Spacer, *Adv. Sci.*, 2023, **10**, 2301149.

22 H. Rong, Y. Ma, Y. Liu, Q. Fan, W. Li, X. Zhao, L. Wei, J. Luo and Z. Sun, Tailoring a Two-Dimensional Halide Perovskite Composed of the Secondary Amine Cation for Anisotropic X-ray Responses, *Inorg. Chem.*, 2024, **63**, 11340–11346.

23 Y. Ma, W. Li, Y. Liu, W. Guo, H. Xu, S. Han, L. Tang, Q. Fan, J. Luo and Z. Sun, X-ray-Induced Pyroelectric Effect in a Perovskite Ferroelectric Drives Low Detection Limit Self-Powered Responses, *ACS Cent. Sci.*, 2023, **9**, 2350–2357.

24 Y. Jiang, C. Zhang, Z.-K. Zhu, J. Wu, P. Yu, Y. Zeng, H. Ye, H. Dai, R. Li, Q. Guan, G. Chen, H. Yang and J. Luo, Multi-axial Self-driven X-ray Detection by a Two-dimensional Biaxial Hybrid Organic-Inorganic Perovskite Ferroelectric, *Angew. Chem., Int. Ed.*, 2024, **63**(44), e202407305.

25 Y. Li, T. Yang, Z. Xu, X. Liu, X. Huang, S. Han, Y. Liu, M. Li, J. Luo and Z. Sun, Dimensional Reduction of $Cs_2AgBiBr_6$: A 2D Hybrid Double Perovskite with Strong Polarization Sensitivity, *Angew. Chem., Int. Ed.*, 2020, **59**, 3429–3433.

26 Z. Xu, X. Liu, Y. Li, X. Liu, T. Yang, C. JI, S. Han, Y. Xu, J. Luo and Z. Sun, Exploring Lead-Free Hybrid Double Perovskite Crystals of $(BA)_2CsAgBiBr_7$ with Large Mobility-Lifetime Product toward X-Ray Detection, *Angew. Chem., Int. Ed.*, 2019, **58**, 15757–15761.

27 Y. Liu, Y. Ma, X. Zeng, H. Xu, W. Guo, B. Wang, L. Hua, L. Tang, J. Luo and Z. Sun, A high-temperature double perovskite molecule-based antiferroelectric with excellent anti-breakdown capacity for energy storage, *Nat. Commun.*, 2023, **14**, 2420.

28 M. Ge, S. Chen, X. Fu, Y. Feng, D. Wang and M. Yuan, Effects of Fluorinated Aromatic Spacer in Ag–Bi Double Perovskite for X-ray Detector, *J. Mater. Chem. C*, 2022, **126**, 19417–19423.

29 Z. K. Zhu, T. Zhu, J. Wu, S. You, P. Yu, X. Liu, L. Li, C. Ji and J. Luo, Discovering New Type of Lead-Free Cluster-Based Hybrid Double Perovskite Derivatives with Chiral Optical Activities and Low X-Ray Detection Limit, *Adv. Funct. Mater.*, 2023, **33**, 2214660.

30 C. F. Wang, H. Li, Q. Ji, C. Ma, L. Liu, H. Y. Ye, B. Cao, G. Yuan, H. F. Lu, D. W. Fu, M. G. Ju, J. Wang, K. Zhao and Y. Zhang, Discovery of a 2D Hybrid Silver/Antimony-Based Iodide Double Perovskite Photoferroelectric with Photostrictive Effect and Efficient X-Ray Response, *Adv. Funct. Mater.*, 2022, **32**, 2205918.

31 Z. Xu, H. Wu, D. Li, W. Wu, L. Li and J. Luo, A lead-free I-based hybrid double perovskite $(I\text{-}C_4H_8NH_3)_4AgBiI_8$ for X-ray detection, *J. Mater. Chem. C*, 2021, **9**, 13157–13161.

32 J. Wu, S. You, P. Yu, Q. Guan, Z.-K. Zhu, Z. Li, C. Qu, H. Zhong, L. Li and J. Luo, Chirality Inducing Polar Photovoltage in a 2D Lead-Free Double Perovskite toward Self-Powered X-ray Detection, *ACS Energy Lett.*, 2023, **8**, 2809–2816.

33 S. You, Z. K. Zhu, S. Dai, J. Wu, Q. Guan, T. Zhu, P. Yu, C. Chen, Q. Chen and J. Luo, Inch-Size Single Crystals of Lead-Free Chiral Perovskites with Bulk Photovoltaic Effect for Stable Self-Driven X-Ray Detection, *Adv. Funct. Mater.*, 2023, **33**, 2303523.

34 W. Guo, H. Xu, Q. Fan, P. Zhu, Y. Ma, Y. Liu, X. Zeng, J. Luo and Z. Sun, Centimeter-Size Single Crystal of a Polar Dion-Jacobson Double Perovskite with Large Mobility-Lifetime Product toward Effective X-Ray Detection, *Adv. Opt. Mater.*, 2024, **12**, 2303291.

35 C. F. Wang, H. Li, M. G. Li, Y. Cui, X. Song, Q. W. Wang, J. Y. Jiang, M. M. Hua, Q. Xu, K. Zhao, H. Y. Ye and Y. Zhang, Centimeter-Sized Single Crystals of Two-Dimensional Hybrid Iodide Double Perovskite $(4,4\text{-Difluoropiperidinium})_4AgBiI_8$ for High-Temperature Ferroelectricity and Efficient X-Ray Detection, *Adv. Funct. Mater.*, 2021, **31**, 2009457.

36 G. Chen, H. Dai, Z. K. Zhu, J. Wu, P. Yu, Y. Zeng, Y. Zheng, L. Xu and J. Luo, Dion-Jacobson Type Lead-Free Double Perovskite with Ultra-Narrow Aromatic Interlayer Spacing for Highly Sensitive and Stable X-ray Detection, *Small*, 2024, **20**, 2312281.

37 Y. Yao, H. Jiang, Y. Peng, X. Zhang, S. Chen, X. Liu and J. Luo, High-Curie Temperature Multilayered Hybrid Double Perovskite Photoferroelectrics Induced by Aromatic Cation Alloying, *J. Am. Chem. Soc.*, 2021, **143**, 15900−15906.

 